SCA2003-19: CO-INJECTED CO_2-BRINE INTERACTIONS WITH INDIANA LIMESTONE

Reid B. Grigg and Robert K. Svec, New Mexico Petroleum Recovery Research Center

This paper was prepared for presentation at the International Symposium of the Society of Core Analysts held in Pau, France, 21-24 September 2003

ABSTRACT

This paper reports findings of coreflooding limestone with co-injected carbon dioxide (CO_2) and brine at reservoir pressure and temperature. Metal chlorides were added as tracer components to the injection brine and appeared in quantities well above natural levels in deposited carbonates. Core segment porosity and permeability are reported to indicate dissolution and deposition. Finally, the core was sectioned and analyzed by chemical and back-scattered electron imaging (BSEI) and chemical titration for compositional changes.

Porosity and permeability increased and decreased corresponding to suspected dissolution and precipitation. Qualitative and quantitative analyses confirmed the deposition of trace metals within deposited carbonate material, providing direct evidence of deposition. These phenomena can occur during CO_2 injection into carbonate geological formations, whether for improved oil recovery (IOR) or greenhouse gas sequestration. With IOR the concern is for injectivity changes, while the issues for sequestration are long-term storage capacity and seal integrity.

INTRODUCTION

Injectivity abnormalities in water-alternating-gas (WAG) IOR processes seem to mystify the petroleum industry [1]. A survey on CO_2 flooding indicated that loss of injectivity on WAG cycles is a crucial limiting factor in many projects [2]. Based on the fluid flow properties of CO_2, one intuitively expects gas injectivity to be greater than the waterflood brine injectivity [3]. However, in practice, this behavior is not always observed. Also, water injectivity during WAG cycles has been reported to be higher in some projects [4-8] and lower in other projects [9-12] than waterflood injectivity. It is perplexing that some reservoirs lose injectivity and others increase injectivity after the first slug of CO_2 is injected, and that this phenomenon may occur on a local or field-wide scale. Injection wells in the same field and reservoir may behave with significant difference. The change of injectivity has been investigated in the laboratory by several research groups with mixed results [6,13,14]. Change in rock properties due to fluid/rock interactions can account for some of the field injectivity behavior [15-18].

Following injection, some mineral or aqueous trapping may occur [19], transforming CO_2 into less mobile forms and possibly decreasing permeability in some areas of the reservoir, thus providing permanent sequestration. However, at least near the wellbore, as in-situ pH decreases and the water is undersaturated in many components such as

carbonates, dissolution of the rock matrix is likely to occur, increasing permeability and thus fluid mobility. Inversely, deposition may occur as the fluid proceeds through the reservoir, which becomes saturated. Reservoir pressure subsequently decreases, reducing solubility in the brine. This can result in reduced permeability and CO_2 mobility. One motivation for this study is to gather information that can be used to calibrate and verify aspects of a new reactive transport model. This model and some of the preliminary results have been previously discussed in publications and presentations [20,21].

In earlier work quarried Indiana (Salem) limestone core was tested in order to investigate the relationship between WAG fluids and the formation rock [14]. Pressure transient data was collected from these cores for calculation of permeability and injectivity. Coreflooding was conducted in the WAG sequence at in-situ conditions. BSEI was performed on pre- and post-flood samples to detect changes in the cores. Macroscopic and microscopic dissolution features were observed in all cores exposed to WAG fluids. Carbonate dissolution caused changes in core permeability and porosity.

In the earlier study, carbonate deposition was indicated by permeability decreases downstream and suggested by the depositional structures seen using BSEI [14]. This is discussed in some detail in the earlier study, but results were not satisfactory because the compositions of the original rock and apparent deposits were essentially identical [14]. In the present study the brine has been modified with components that form carbonates and are found as trace impurities in limestone. These will aid in quantifying fluid-mineral interactions by providing a compositional contrast between the original rock and any new deposits.

PROCEDURES

Indiana limestone, a bioclastic grainstone composed primarily (>99%) of calcite (calcium carbonates, $CaCO_3$), was used in the coreflood experiment. This rock has sufficient permeability and porosity for our laboratory measurements and is a compositionally simple carbonate rock. The apparatus (shown in Fig. 1) used for the coreflooding experiments is similar to the one used in previous work [14]. Selected reservoir conditions were 100ºF and a minimum (core outlet) pressure of 2000 psig. These conditions, used in previous experiments, are similar to conditions in many Permian Basin Reservoirs [14]. Both are above the critical conditions of CO_2 and are in a pressure-temperature region where physical conditions do not change rapidly with respect to temperature or pressure, and physical parameters are similar to liquid CO_2.

The flooded core was a composite core composed of two sequential pieces of Indiana limestone, referred to as segment A and segment B. The fluid inlet was located on segment A, segments A and B were in direct contact, and the fluid outlet was located on segment B. To insure a good seal of the core sleeve and to force the two core segments into close contact an overburden (radial and axial) pressure of 4000 psig was maintained with an effective stress of about 2000 psi. No foreign material such as filter paper was placed between the two core segments to promote capillary contact because previous

experience during corefloods of long duration saw contact material degrade and cause surface plugging. Also, dissolution at the segment juncture appeared to be continuous across the two core segments with no visual discontinuities due to the juncture.

Physical parameters of the core segments are listed in Table 2. The injection scheme was a constant ratio (1:1) brine with CO_2 co-injection. The initial combined flow rate was 80cc/hr (18.28ft/d), but was reduced to 40cc/hr (9.14ft/d). The cores were periodically cleaned with tetrahydrofuran and dried, then removed from the core holder for inspection and brine permeability and porosity measurements. Tetrahydrofuran is used for its properties that enable removal of both aqueous and hydrocarbon phases with one application without dissolution of inorganic core material. Finally, the core was reassembled into the same orientation, whole core brine permeability determined, and the co-injection of brine and CO_2 continued. The whole core brine permeability was also determined before the first co-injection.

The brine formula used in the experiment was composed of five salts, all chlorides, with composition as listed in Table 1. The brine total dissolved solids (tds) of 30,000 ppm was used with emphasis on selected trace metals: manganese (Mn), magnesium (Mg), and strontium (Sr). They are each known to occur in calcite as impurities (see fresh core analysis in Table 3). 30,000 ppm tds brine was selected to represent typical Permian Basin waterflood brine. The exact composition was 10,000 ppm sodium chloride (NaCl) with 5,000 ppm each of Ca, Mn, Mg, and Sr chlorides. These were selected to have equal concentration as a first attempt to test the concept of trace metals in any carbonate precipitate. By BSEI and quantitative measurements the locations along the core that were enriched with respect to these elements could be identified. BSEI would allow us to identify the mode of deposition on the original rock matrix.

RESULTS

Core Flood Data Trends

Over the course of the experiment, 15.1 liters of each phase (brine and CO_2) were co-injected; the total volume of fluid co-injected was 30.2 liters. An additional 5 liters of brine was used in single-phase injection during CO_2 desaturation and brine permeability and porosity measurements. Since the original pore volume of the core totaled 195 cc, these yields a total of 155 pore volumes (PV) of fluid co-injected.

Measurable changes occurred in the permeability and porosity of both core segments. Figure 2 shows the trend in core porosity. Note that both core segments show an initial decrease in porosity until about 55 PV injected, when porosity begins to increase. This interval corresponds to the injection of a combined rate of 80 cc/hr. The change was strongest in segment A, which is the upstream side of the composite core. The pore space of segment A was observed to decrease from 57.64 cc to 53.61 cc (-7.0%) during the first 55 PV of injection. During the same period the pore space of segment B decreased from 137.2 cc to 129.72 cc (-5.5%). During the next 100 PV of co-injection (55 PV to 155 PV), at a combined injection rate of 40 cc/hr, porosity was observed to increase in both

core segments. Pore space in segment A increased substantially from 53.61 cc to 66.9 cc (+24.8%) and pore space in segment B increased modestly from 129.72 cc to 135.54 cc (+4.5%).
Core permeability to brine is shown in Fig. 3. Permeabilities of individual segments A and B were unavailable until midway through the experiment because of instrumental failures during the first interval of data acquisition. However, the whole core permeability decreased monotonically during the first half of the experiment. During the early part of the flood, while whole core permeability was decreasing, the formation of a solution channel was observed at the injection face during periodic visual inspection of the core. The solution channel is shown in Fig. 4. At 10 PV co-injected the core inlet surface on segment A was slightly roughened by dissolution of the co-injected fluids. When the core was inspected after 56 PV of co-injection a small solution channel had begun to form, apparently extending only several millimeters into the core. By 84 PV of co-injection a solution channel was clearly established, extending tortuously into the core and out of view. Termination of the experiment was triggered by the very high permeability of 1978 md measured on segment A after 155 PV of co-injection.

Upon sectioning the flooded core the channel was found to extend nearly to the end of segment A. Figure 5 shows the longitudinally sectioned core segments. Flow direction is indicated on the figure by the arrows. The tortuous path of the solution channel is clearly visible in segment A. Near the end of the channel it appears to broaden and terminate into a region of solution enhanced porosity that extended to the end of segment A. On the adjacent face of segment B there also appears to be a region (highlighted by the oval) of solution-enhanced porosity. These two regions were in contact when the core segments were installed in the core holder during flooding. There are no visible solution or deposition features in the remainder of segment B.

The permeability plot (Fig 3) shows that the composite core and segment permeabilities during the mid-run times were decreasing while a solution channel (an intrinsically very high permeability feature) was progressing through segment A into the first of segment B (Fig 5). Therefore another process was taking place simultaneously, which was capable of reducing core permeability in part of the core while the process of dissolution was increasing permeability in another part. Factors that might have affected core permeability in this way are fines migration with pore plugging or occlusion of pores by the deposition of new mineral material. The introduction of any foreign external particles was prevented by filters (0.5 μ) at the core inlet.

Chemical and BSE Analysis
The sectioned core segments were sampled by removing 0.5 in. diameter core plugs at a point 1 cm from the inlet face and at regular 5 cm intervals thereafter to the outlet face of the core. Each core plug was cut in half, with one piece used for the chemical analysis and the other used for BSEI. Chemical samples were pulverized to powder and dissolved in acid, then analyzed by the inductively coupled plasma–mass spectrometer (ICP-MS) method for Mg, Mn, and Sr. Samples were analyzed for Ca by EDTA titration. Fresh

rock samples trimmed from the core segments before flooding were used to establish baseline rock properties. The results of the chemical analysis are presented in Table 3.

There is no significant trend in the Ca and Mg data. The data for Mn and Sr are plotted in Fig. 6. The Mn values are elevated up to 500 times above the baseline. The trend peaks at 15 cm and trails off toward the end of the core. This trend is also seen in the Sr data. The Sr peak is about twice the baseline and also occurs at 15 cm and trails off toward the end of the core. In the case of Mn and Sr the peaks correspond, within sampling spatial resolution, to the final position of the solution channel, which had reached approximately 17 cm into the core at the end of the coreflooding experiment.

The post-flood chemical quantitative data obtained by BSEI is found in Table 4 and is presented with pre-flood composition data of original core using ICP-MS and BSEI methods. At several distances in the sectioned core the sample was surveyed and several point (10 to 20 micron diameter) measurements were averaged to obtain the table entry. The flooded core data is separated into two parts: those regions which appear identical with the original rock texture and those that appear to be newly deposited material by virtue of a significant contrast in atomic number (Z). As seen in the table, this contrast in Z is caused primarily by strong enrichment with respect to Mn and secondarily, Sr.

The distribution of the deposited material is shown in the BSEI images Figs. 7 and 8. Figure 7 shows a wide view of the rock matrix on the sample taken from the flooded core 15 cm from the injection face. The calcite grains and cement appear as grey, pore space is black, and the new Mn-rich deposits are white. The new deposits are scattered throughout the region and show a tendency to form at grain boundaries rather than on the cement walls in the larger pores. Figure 8 shows a higher magnification image of the sample taken from 35 cm from the injection face. This deposit has formed on the calcite cement (grey) rather than a grain. It can be clearly seen that the deposit shows essentially the same euhedral growth structure that is evident in the cement. Also a zonation in the deposit due to a contrast in the Mn/Ca ratio during growth is distinctly visible. The inner areas with a higher Mn to Ca content appear brighter than the rims.

DISCUSSION

In an earlier paper [14], we reported that dissolution could be seen on a macroscopic as well as microscopic scale. Deposits downstream were evident from decreased permeability and what appeared to be fresh deposits viewed using BSEI. Suspected deposits with composition and structures similar to the original carbonates were therefore not diagnostic. The Mn and Sr carbonate are more and less soluble in brine, respectively, than is calcite. The purpose of the tracer components was to provide a compositional contrast to the original limestone in new deposits.

The porosity and permeability of the system decreased at first, and then increased above the original value by the end of the flood. For segment A the porosity and permeability became much higher by the end of the tests. A solution channel developed in segment A.

The evolution of the solution channel entrance is shown in Fig. 4 at three different times during the test as a function of PV injected. This, with the increasing roughness at the injection surface, shows dissolution. The full extent of the dissolution was revealed when segments A and B were cut longitudinally after termination of the experiment (Fig. 5). The solution channel advanced most of the distance across segment A. The beginning of some apparent dissolution is seen near the injection face of segment B.

Results of BSEI identification in Table 4 show a contrast in core properties between pre-flood and post-flood states. Within the post-flood core are areas of original rock texture (no detectable alterations) and new deposits. In Fig. 8 the new deposits show as white or high Z areas and the original rock (grain and cement) as grey. Mg and Ca concentrations in the new deposits were less than half the concentration in the original core. Mn concentrations increased by at least three orders of magnitude and Sr increased 4–8 times in the new deposits. The apparent enrichment of the post-flood original rock texture with respect to Mn, seen in Table 4, may be caused by the sampling method when the BSI microscope was used in the quantitative mode. The instrument is capable of measuring composition in 20, 10, or 5 micron diameter circles that are chosen at certain coordinates on the sample as images are obtained. Many of the features of interest were little larger then the sampling area which could be used. Repeatability of the BSE coordinate system was a factor in several measurements, for instance when a measurement of the rock matrix returned less than 100% mass in the sample area it was obvious that the instrument had included some pore space. However, if the sample area inadvertently include some adjacent but contrasting grain this error is less obvious

An active area of deposition at the leading edge of the solution channel was indicated when simulating calcite dissolution and deposition using a transport-reactive model [20, 21]. This corresponds to the measured Mn and Sr peaks in the vicinity of the termination of the solution channel, see Fig. 6 and Table 3. This is supported by the BSEI images, where the abundance of high Z deposits increases from the injection face, peaking at about 15 cm and then decreases to the end of the core system.

Using the 15 cm value for the deposit composition would yield a molar composition of about 66% Mn-carbonate, see Table 4. If the total composition at 15 cm is taken to be 8.9% Mn-carbonate, see Table 3, then the new deposit would represent about 13.5% of the total carbonates at this point in the core. If there had been no dissolution in this area this would indicate a reduction of porosity to about 6% of total volume from the original of about 17%. This is the most likely cause of permeability reduction across the core, even though major dissolution is occurring upstream in the core.

As discussed earlier, injectivity increases and decreases occur in field WAG projects. The dissolution and deposition seen in this study are possible mechanisms for these changes. An unanticipated aspect of this work is the discovery that significant deposition can be occurring in the vicinity of major dissolution. The scaling aspect of this work to the reservoir has not yet been considered. The processes occurring within centimeters may

translate to tens of meters in the reservoir, dependent on the scaling of pressure and chemical gradients.

CONCLUSIONS

1. Dissolution of carbonates at reservoir conditions during co-injection of CO_2 and brine was confirmed visually, and by porosity and permeability increases.
2. Deposition of carbonates was indicated by porosity and permeability reduction.
3. Deposition was determined by BSEI identification of high Z areas and reached a maximum near the end of the solution channel.
4. The composition of deposits was strongly influenced by the tracer brine composition.
5. Deposition and dissolution were found to occur in close proximity.

ACKNOWLEDGEMENTS

The authors acknowledge the financial support of the US Department of Energy (contract no. DE-FC26-01BC-15364) and the State of New Mexico and the assistance of Lynn Brandvold (analytical) and Lynn Heizler (BSEI) of the New Mexico Bureau of Geology.

REFERENCES

1. Rogers, J. D. and Grigg, R.B.: "A Literature Analysis of the WAG Injectivity Abnormalities in the CO_2 Process," *SPERE*, Oct. 2001, 375-386.
2. Grigg, R.B. and Schechter, D.S.: "State of the Industry in CO_2 Floods," SPE 38849 presented at the 1997 SPE ATCE, San Antonio, Oct. 6-9.
3. Hadlow, R.E.: "Update of Industry Experience with CO_2 Injection," SPE 24928 presented at the 1992 SPE ATCE, Washington D.C., Oct. 4-7.
4. Winzinger, R., *et al*.: "Design of a Major CO_2 Flood, North Ward Estes Field, Ward County, Texas," *SPERE* (Feb. 1991) 11.
5. Ring, J.N. and Smith, D.J.: "An Overview of the North Ward Estes CO_2 Flood," SPE 30729 presented at the 1995 SPE ATCE, Dallas, Oct. 22-25.
6. Prieditis, J., *et al*.: "A Laboratory and Field Injectivity Study: CO_2 WAG in the San Andres Formation of West Texas," SPE 22653 presented at the 1991 SPE ATCE, Dallas, Oct. 6-9.
7. Christman, P.G., and Gorell, S. B.: "A Comparison of Laboratory and Field-Observed CO_2 Tertiary Injectivity," SPE 17335 presented at the 1988 SPE/DOE Enhanced Oil Recovery Symposium, Tulsa, April 17-20.
8. Good, P.A. and Downer, D.G.: "Cedar Creek Anticline Carbon Dioxide Injectivity Test: Design, Implementation, and Analysis," SPE 17326 presented at the 1988 SPE/DOE Enhanced Oil Recovery Symposium, Tulsa, April 17-20.
9. Henry, R.L., *et al*.: "Utilization of Composition Observation Wells in a West Texas CO_2 Pilot Flood," SPE 9786 presented at the 1981 SPE/DOE Enhanced Oil Recovery Symposium, Tulsa, April 5-8.

10. Patel, P.D., *et al.*: "An Investigation of Unexpectedly Low Field-Observed Fluid Mobilities during Some CO_2 Tertiary Floods," SPE 14308 presented at the 1985 SPE ATCE, Las Vegas, Sept. 22-25.
11. Potter, G.F.: "The Effects of CO_2 Flooding on Wettability of West Texas Dolomitic Formations," SPE 16716 presented at the 1987 SPE ATCE, Dallas, Sept. 27-30.
12. Schneider, F.N., and Owens, W. W.: "Relative Permeability Studies of Gas-Water Flow Following Solvent Injection in Carbonate Rocks," *SPEJ* (Feb. 1976) 23.
13. Kamath J., *et al.*: "Laboratory Investigation of Injectivity Losses During WAG in West Texas Dolomites," SPE 39791 presented at the 1998 SPE Permian Basin Oil and Gas Recovery Conference, Midland, March 25-27.
14. Svec, R.K. and Grigg, R.B.: "Physical Effects of WAG Fluids on Carbonate Core Plugs," SPE 71496 presented at the 2001 SPE ATCE, New Orleans, Sept. 30–Oct. 3.
15. Ross, G.D., *et al.*: "The Dissolution Effects of CO_2-Brine Systems on the Permeability of U.K. and North Sea Calcareous Sandstones," SPE 10685 presented at the 1982 SPE/DOE Symposium on Enhanced Oil Recovery, Tulsa, April 4-7.
16. Mathis, R.L. and Sears, S.O.: "Effect of CO_2 Flooding on Dolomite Reservoir Rock, Denver Unit Wasson (San Andres) Field," SPE 13132 presented at the 1984 SPE ATCE, Houston, Sept. 16-19.
17. Sayegh, S.G., *et al.*: "Rock/Fluid Interactions of Carbonated Brines in a Sandstone Reservoir: Pembina Cardium, Alberta, Canada," *SPEFE* (Dec. 1990) 399.
18. Bowker, K.A. and Shuler, P.J.: "Carbon Dioxide Injection and Resultant Alteration of the Weber Sandstone, Rangely Field, Colorado," The American Association of Petroleum Geologists Bulletin, V. 75, No. 9 (Sept. 1991) 1489.
19. Wawersik, R., W., *et al.*: "Terrestrial Sequestration of CO_2: An Assessment of Research Needs," *Advances in Geophysics* **43,** (2001).
20. Wellman, T.P.: *Concatenation of Reactive Transport Model to Simulate CO_2 Sequestration in Geologic Media*, Thesis, New Mexico Institute of Mining and Technology, (2002).
21. Wellman, T.P, *et al.*: "Evaluation of CO_2-Brine-Reservoir Rock Interaction with Laboratory Flow Tests and Reactive Transport Modeling," SPE 80228 presented at the 2003 SPE Oilfield Chemistry Symposium, Houston, Feb. 5-8.

Table 1. Brine Composition

Salt	Conc(ppm)	Molar(M)
NaCl	10000	0.1710
$CaCl_2$	5000	0.0450
$MnCl_2$	5000	0.0397
$MgCl_2$	5000	0.0525
$SrCl_2$	5000	0.0315

Table 2. Initial Core Parameters

	D., cm	L., cm	Por., %	PV, cc
Seg.-A	5.03	17.15	16.91	57.6
Seg.-B	5.03	39.37	17.54	137.2
Core	5.03	56.52	17.35	194.8

Table 3. Chemical Analysis (bulk core)

Pos. [cm]	*Mg [ppm]*	*Ca [ppm]*	*Mn [ppm]*	*Sr [ppm]*	**Pos. [cm]**	*Mg [ppm]*	*Ca [ppm]*	*Mn [ppm]*	*Sr [ppm]*
1	3000	399000	4800	380	**30**	4040	393000	5460	303
5	3390	390000	7370	299	**35**	4070	394000	5080	325
10	3530	389000	14700	353	**40**	3220	393000	3620	282
15	3620	388000	53100	523	**45**	3400	396150	4000	280
20	3470	391000	20800	367	**50**	3370	393000	3170	258
25	3480	400500	6760	307	**55**	3500	392500	3100	289

Table 4. Composition Results by Quantitative BSEI (points in the core)

State	**Texture**	**Position [cm]**	**Mg [ppm]**	**Ca [ppm]**	**Mn [ppm]**	**Sr [ppm]**	**# of points**	**Method**
Pre-flood	Original	NA	3053	391940	43	220	4	ICP-MS
Pre-flood	Original	NA	2364	396256	119	237	24	BSE
Post-flood	Original	5	1597	401479	82	211	4	BSE
Post-flood	Original	15	1953	401845	1393	109	7	BSE
Post-flood	Original	25	2717	393447	1279	235	14	BSE
Post-flood	Original	35	1591	404066	1354	101	3	BSE
Post-flood	Original	55	2926	397165	241	402	3	BSE
Post-flood	Deposit	5	1240	140821	302176	1721	3	BSE
Post-flood	Deposit	15	1096	119559	325784	1662	14	BSE
Post-flood	Deposit	25	951	97577	349775	1662	9	BSE
Post-flood	Deposit	35	721	105826	334769	1662	4	BSE
Post-flood	Deposit	55	1297	169289	224613	1424	4	BSE

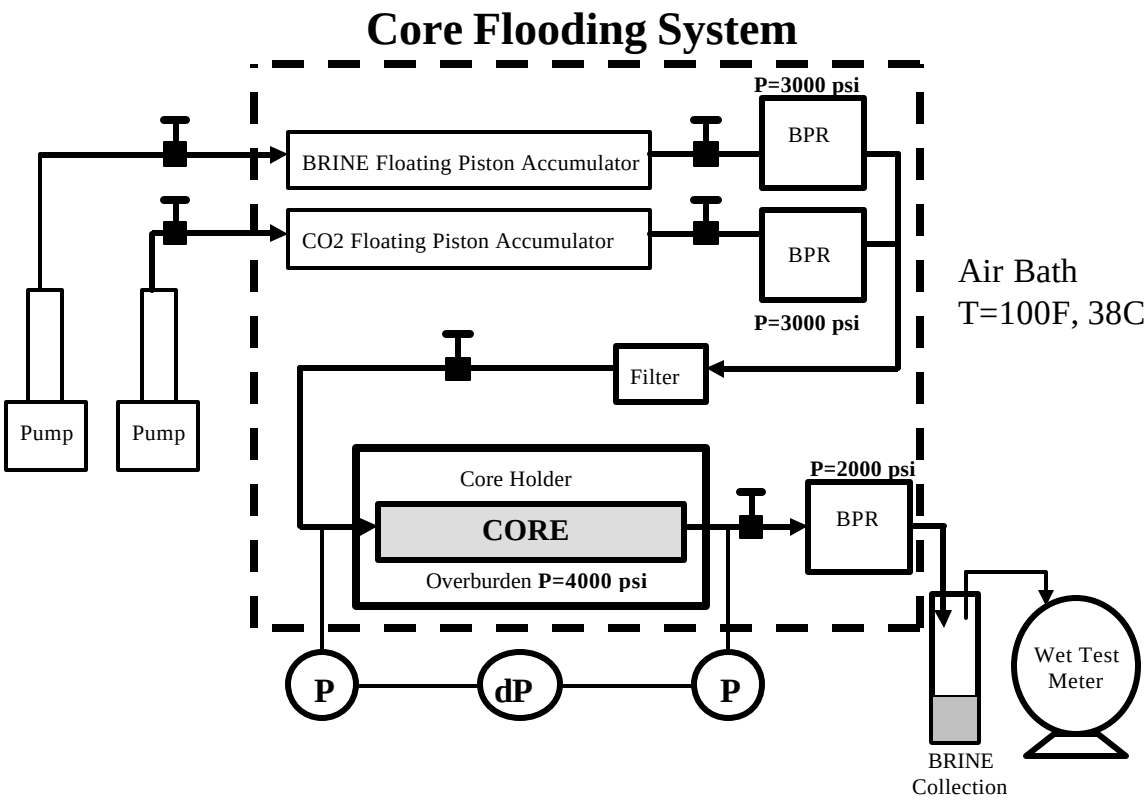

Fig. 1. The core flooding apparatus.

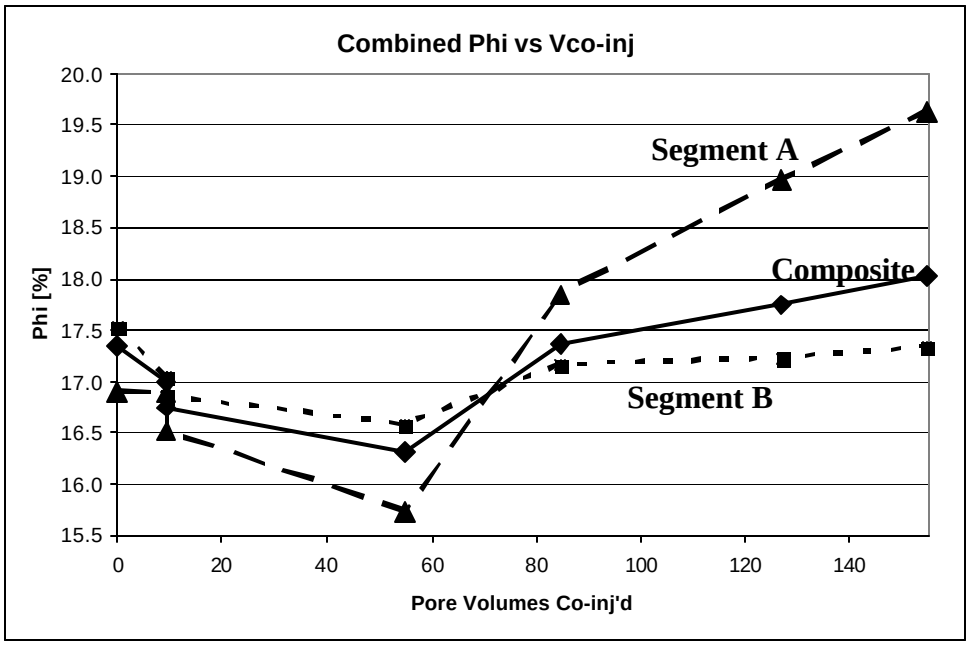

Fig. 2. Core porosity.

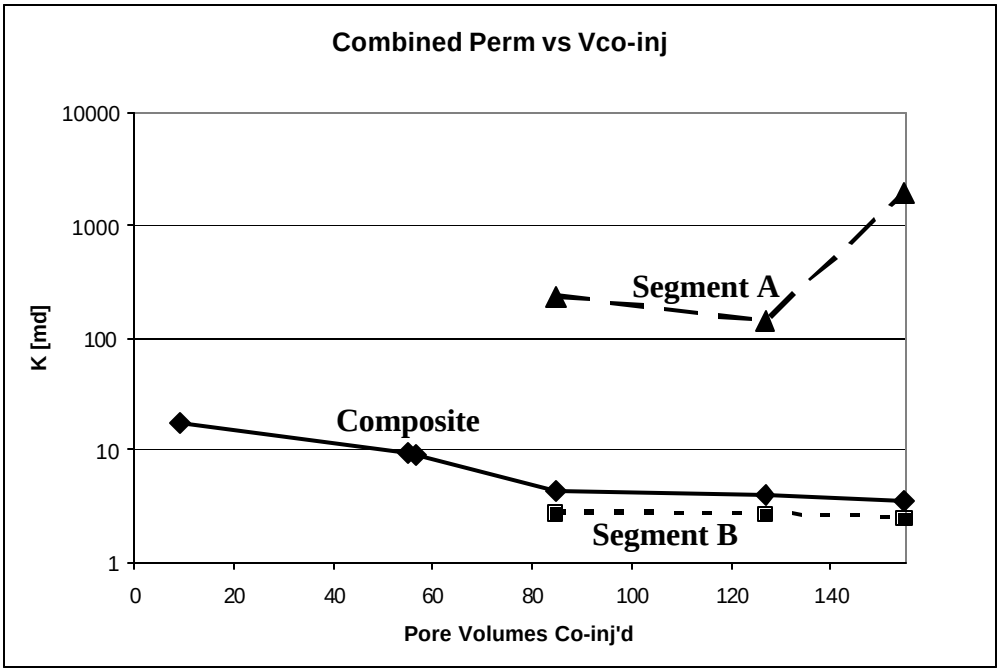

Fig. 3. Core permeability.

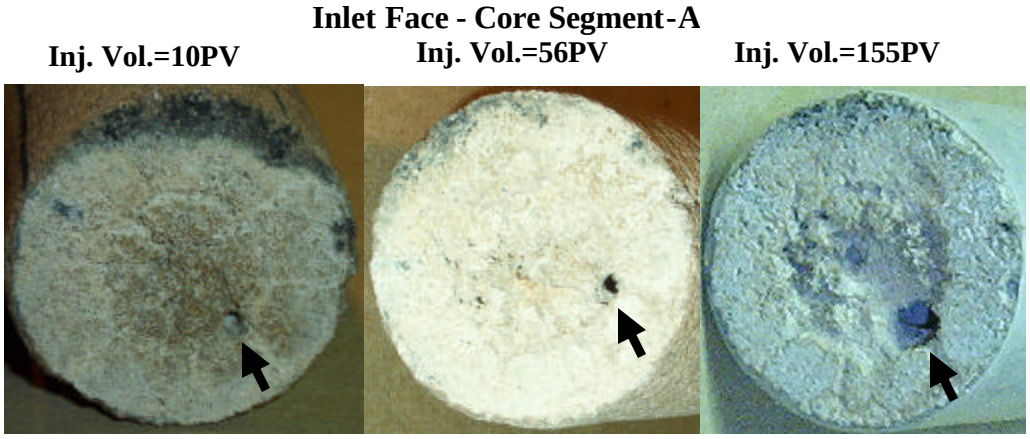

Fig. 4. Solution channel progress at the injection face vs. pore volumes injected.

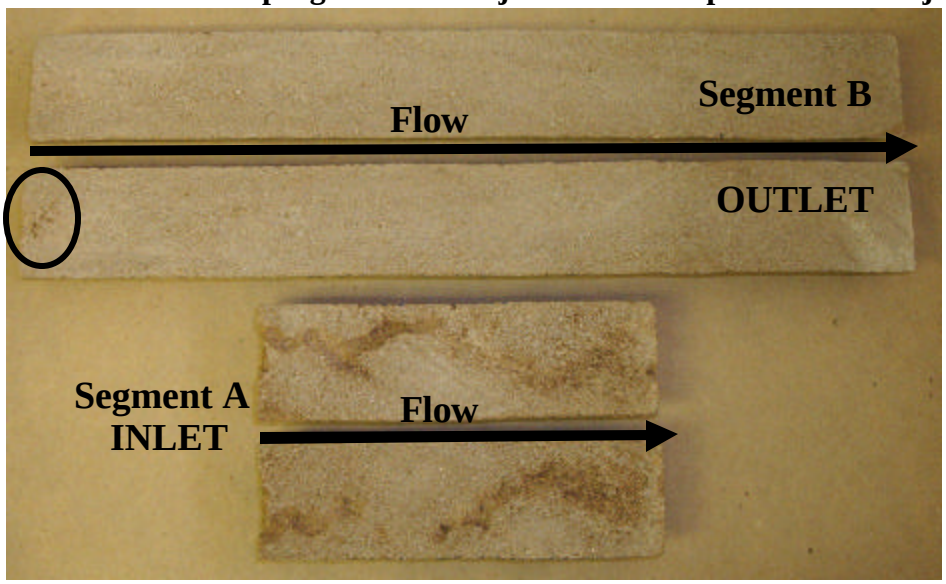

Figure 5. Core segments cut in half longitudinally after the end of the flood.

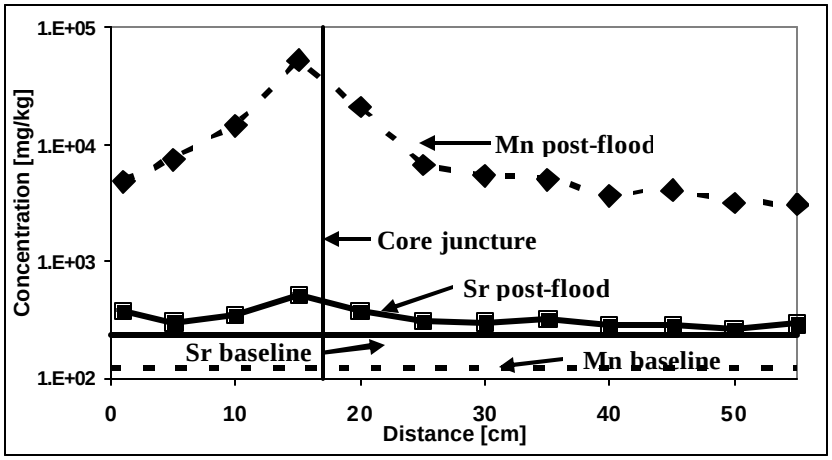

Fig. 6. Composition of Mn. and Sr. along the core length at the end of the flood.

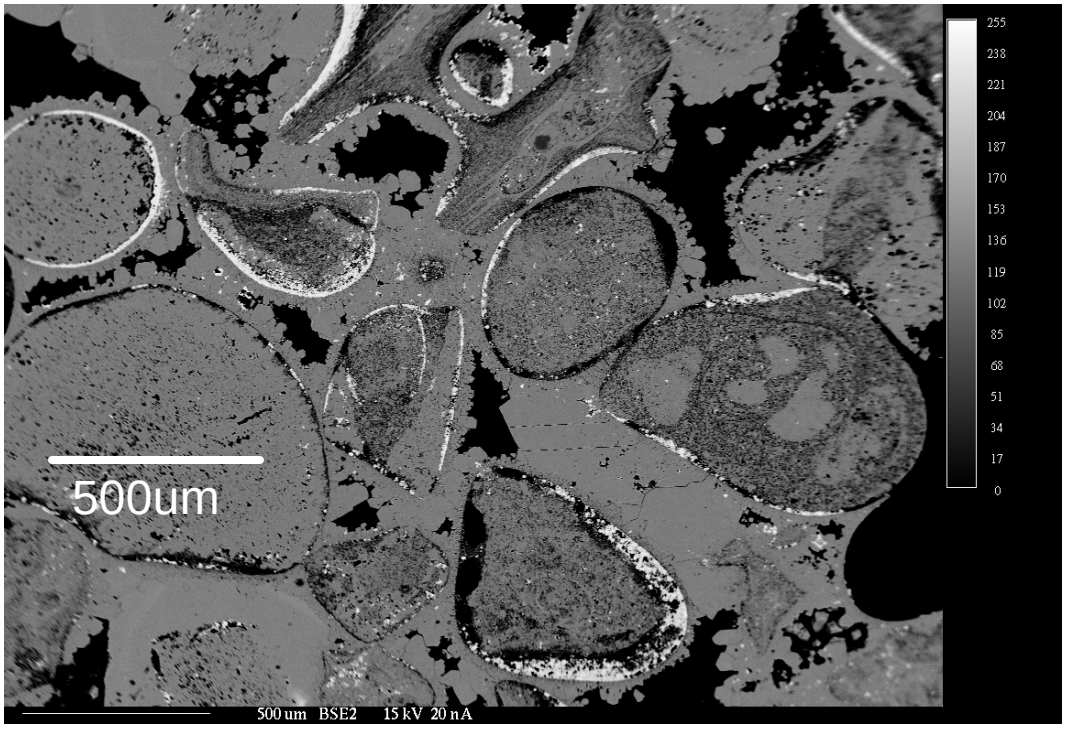

Figure 7. BSEI wide view at 15cm into the flooded core.

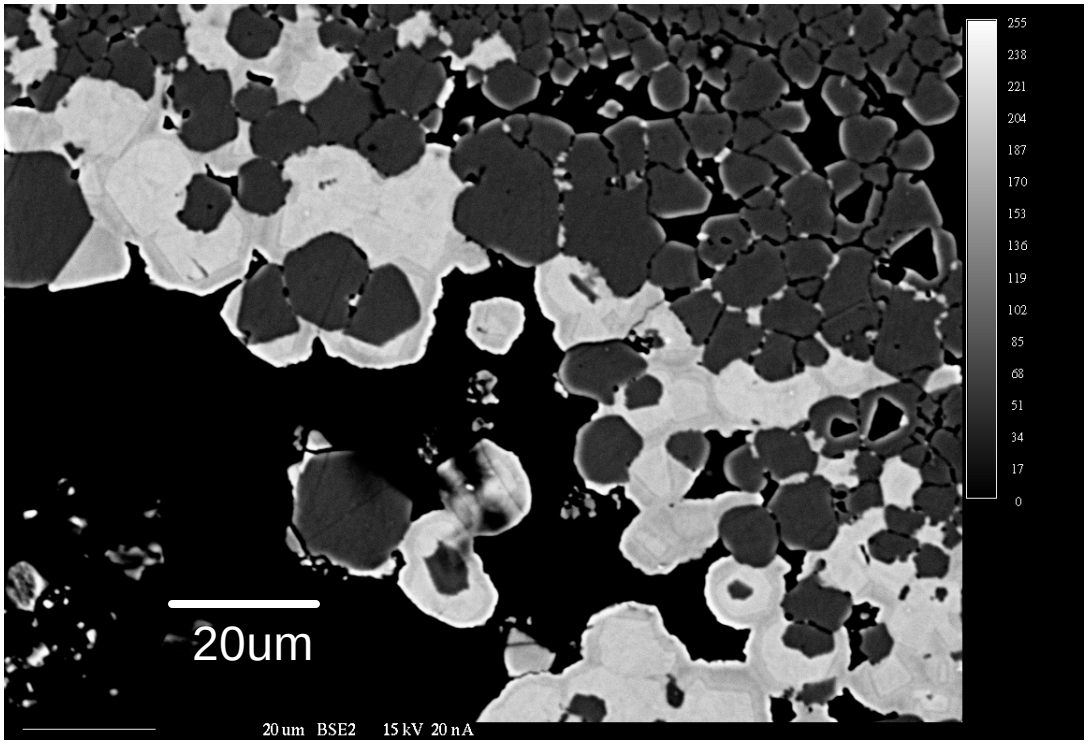

Fig. 8. New growth at 35 cm into the core. Zonation can be seen.